Heliyon 10 (2024) e36087

Contents lists available at ScienceDirect

Heliyon

journal homepage: www.cell.com/heliyon

Research article

Effect of powder composition, PTAW parameters on dilution, microstructure and hardness of Ni–Cr–Si–B alloy deposition: Experimental investigation and prediction using machine learning technique

Venkatesh Chenrayan [a,**], Kiran Shahapurkar [b,c], Chandru Manivannan [d], L. Rajeshkumar [a,*], N. Sivakumar [e], R. Rajesh sharma [e], R. Venkatesan [f]

[a] AU-Sophisticated Testing and Instrumentation Centre (AU-STIC) and Department of Mechanical Engineering, Alliance School of Applied Engineering, Alliance University, Bengaluru, 562106, India
[b] Centre of Molecular Medicine and Diagnostics (COMManD), Saveetha Dental College and Hospitals, Saveetha Institute of Medical and Technical Sciences, Saveetha University, Chennai, 600077, India
[c] Department of Mechanical Engineering, Faculty of Engineering, University of Malaya, Kuala Lumpur, 50603, Malaysia
[d] Department of Mechanical Engineering, Dhirajlal Gandhi College of Technology, Salem, India
[e] Department of Computer Science Engineering, School of Advanced Computing, Alliance University, Bengaluru, India
[f] Department of Mechanical Engineering, SRM-TRP Engineering College, Tiruchirapalli, India

ARTICLE INFO

Keywords:
Chromium boride
Dilution
Grain growth
Heat affected zone
GRA
Machine learning

ABSTRACT

The implementation of hard-facing alloy on the existing materials caters the need for high-performance surfaces in terms of wear and high temperatures. The present research explore the effect of Plasma Transferred Arc Welding (PTAW) parameters and powder composition on dilution, microstructure and hardness of the commonly used hard-facing alloy Ni–Cr–Si–B powder. The hard-facing alloy was deposited with three weight proportions of boron (2.5 %, 3 % and 3.5 %). The statistical-based Grey Relational Analysis (GRA) followed by a Machine Learning Algorithm (MLA) was implemented to identify the ideal parameters and degree of significance of each parameter and for the prediction of the responses. The dilution percentage, microstructure analysis, and phase detection were estimated through elemental analysis, Scanning electron Microscopy (SEM) and X-ray Diffraction Analysis (XRD) respectively. The experimental and modelling results revealed that 400 mm/min of scanning speed, 8 gm/min of powder delivery, 14 mm of stand-off distance, and 120 A of current were the optimal parameters along with 3.5 wt% of boron powder composition to yield a better dilution, microstructure and hardness.

* Corresponding author.
** Corresponding author.
E-mail addresses: venkyachvsh@yahoo.co.in (V. Chenrayan), Kiranhs1588@gmail.com (K. Shahapurkar), mechchandru123@gmail.com (C. Manivannan), lrkln27@gmail.com (L. Rajeshkumar), drsivakumar.nadarajan@gmail.com (N. Sivakumar), sharmaphd10@gmail.com (R. Rajesh sharma), vengow@gmail.com (R. Venkatesan).

https://doi.org/10.1016/j.heliyon.2024.e36087
Received 24 June 2024; Received in revised form 9 August 2024; Accepted 9 August 2024
Available online 13 August 2024

1. Introduction

The inevitable and extensive industrial applications in different spectrums pose a threat to a material surface to resist high-temperature wear and corrosion environment during its service tenure [1,2]. Conventional material surfaces are no longer capable of performing better in these circumstances [3–5]. The introduction of a hard face over the conventional surface is the recently emerged solution that evolved from surface engineering sciences [6,7]. The secondary hard surface is usually deposited from Cobalt-based stallite alloy [8], carbide-based tungsten [9] or chromium carbide alloy [10], Ni-based colmonoy alloy [11–13], tool steel alloy [14], and titanium-based alloy [15,16]. However, weld overlay (weld cladding) [17], thermal spray [18], clad plate rolling [19], explosive bonding [20], diffusion bonding [21], roll bonding [22] Electroplating is a common technique for depositing metal over metal. Ni–Cr–Si–B alloy is commonly known as colmonoy alloy, which performs excellently in high-temperature wear and corrosion environments [23,24]. The phase transformation of chromium carbides and borides during this deposition is found to be a pivotal agent for the strengthening mechanism [25]. The deposition of colmonoy alloy usually follows either through laser cladding or PTA (Plasma Transferred Arc) cladding [25,26]. The crack formation and its propagation of hard chromium boride have been reported [27–29] owing to the rapid cooling integrated with laser processing. The crack formation and greater restriction in layer deposition are primary drawbacks associated with laser cladding.

Hemmati et al. [30] attempted to deposit Ni–Cr–Si–B by modifying the alloy with the inclusion of 2 and 5 % vanadium to minimize the crack formation during rapid cooling of laser processing. The authors stated that the cracking tendency of the deposited layer was minimised at the cost of hardness loss and that the incorporation of vanadium did not provide any benefit in terms of grain or microstructural refinement. Sudha et al. [31] executed a Ni–Cr–Si–B alloy deposition on AISI 304 L stainless steel using PTA (Plasma Transferred Arc) weld overlay. The interface dilution, morphology of secondary phase transformation, elemental redistribution at the juncture of coating and substrate, and formation of different phases after the deposition were studied using appropriate techniques. The report concluded that interface integrity was attained at a minimum thickness of 760 μm with dilution of mutual elements from coating and substrate. The higher hardness was observed at the surface of the coating and the linear drop in hardness was also observed from the edge of the coating to the point of interface. Chao Zhang et al. [32] conducted a metallurgical examination, hardness and wear evaluation on Ni–Cr–Si–B coated copper substrate. The declaration continues that a significant dilution at the level of 15.9 % was achieved and the hardness and wear resistance were improved 7.8 and 5 times than that of copper substrate. The secondary phases such as chromium boride and chromium carbide were the predominant catalyst in the escalation of hardness and wear resistance. Tian-guo Guan [33] deposited a Ni–Zr–B_4C powder on the SA-283C steel plate through PTA weld overlay method. The microstructural study revealed that the formation of Zirconium boride (ZrB_2 and carbide (ZrC) prompted the coating surface to reach its maximum hardness of 1522 HV, and the authors realized that a greater improvement in wear resistance of 15 times than that of the substrate. However, the authors claimed a better bonding without any evaluation of interface integrity at the interface.

Hemmati et al. [34] developed a Colmonoy alloy hard-facing coating on carbon steel substrate through IPG fiber laser cladding technique by varying the Fe content in the powder to achieve a higher dilution. The dilution was controlled from 5 % to 35 % with an appropriate Fe content in the powder from 8 % to 39 % wt. The dilution was measured through EDS. The report revealed that the increased dilution with increased content of Fe deteriorates the hardness value. The increased Fe content was found to suppress the precipitates of primary chromium boride, and in turn, diminishment in hardness was recorded. The effect of PTA weld overlay parameters on the dilution and bead continuity was investigated by Mandal et al. [35] while they attempted to deposit SS304L powder on SS316 plates. The chief welding parameters like scanning speed, welding current, welding torch distance, and powder feed rate were considered to be parameters and were maintained at six different levels. The effect of each parameter was discussed in detail by keeping other parameters constant. The experimental results manifested that the scanning speed and powder delivery influenced the dilution and bead continuity, whereas welding torch distance did not influence the dilution much. However, a significant mitigation in dilution was observed with the change in welding current.

1.1. Significance of the study

The provision of hard facing layer on the conventional material to enhance the performance against wear and high-temperature working environment is an emerging technique. However, deposition objectives like microstructure changes, dilution, and hardness are the key outcomes availed through precise mitigation of metal cladding parameters. This research utilizes a commonly available colmonoy power to deposit over the AISI 321 steel through PTA weld overlay. However, the deposition of commonly available colmonoy alloy powder and its evaluation of microstructure change and mechanical properties have been reported sufficiently. In contrast, a customized colmonoy alloy powder is proposed to coat in three different variants by modifying the boron content in three levels to promote more boride formation. The novelty and uniqueness present in the study are as follows: 1. Three different levels of boron inclusion to promote more boride formation, 2. Evaluation of the effect of PTA parameters on the key objectives of weld overlay like dilution, microstructure changes and hardness. 3. Prediction of optimal PTA parameters to achieve better microstructure, dilution and hardness through statistical modelling followed by machine learning technique. The effect of powder composition, PTAW parameters on dilution, and microstructure have not been reported so far.

2. Experimental details

2.1. Materials and processes

The commercially available colomnoy alloy (Ni–Cr–Si–B) powder was procured from Metal Mart, Coimbatore, India by customizing the powder's Boron constituent in three different levels as shown in Table 1. The substrate used to deposit the hard-facing alloy was chosen as AISI 321steel whose chemical composition is furnished in Table 2.

PTA 400 model welding resource from Arcraft plasma equipment (India) was pressed into service to deposit the alloy. The specifications of the PTAW 400 are given in Table 3.

Argon gas was utilized as plasma gas and was ionized to generate a high-temperature plasma arc. The non-consumable tungsten electrode was used to initiate the arc to induce high-temperature plasma from the PTA welding unit shown in Fig. 1(a). The powder was fed into the plasma zone where it melted to a molten state for the deposition. The powder particles were transported to the plasma zone through a delivery system equipped with the welding set-up. The tungsten electrode was positioned over the AISI 321substarate shown in Fig. 1 (b) which was preheated to 200^0 C for better bonding. The molten powder was coated on the preheated substrate layer by layer until it reached a thickness of 4 mm and was allowed to cool in an air medium as depicted by Fig. 1(c).

The microstructure formation and its distribution were scrutinized through a scanning electron microscope (FESEM, FEI-Quanta 200). The phase identification was made using XRD (Malvern Panalytical X'pert^3 MRD). The elemental analysis was conducted on the deposited subsurface and interface of deposition-substrate through energy dispersive X-ray spectroscopy (EDAX) (FESEM, FEI-Quanta 200). The hardness of the deposited surface was estimated using Vicker's micro hardness tester (Shimadzu HMV-G 20 DT).

2.2. Experimental design

The chief cladding parameters considered are scanning speed, powder delivery, stand-off distance, and current. Subsequently, the objectives of the experiments considered are dilution, microstructure (chromium boride formation) and hardness. The PTA welding process parameters are followed in three distinguished levels such as low, medium and high to investigate the influence of cladding parameters over the objectives regarded. Table 4 depicts the list of parameters and their levels maintained for the experimental deposition [35,36]. Taguchi's design of experiments was enforced to arrive at an orthogonal array of combinations of experimental runs. As per the L18 orthogonal array, 18 experiments were conducted and the corresponding observations of three objectives are tabulated in Table Table 5.

The dilution is the indicator of good penetration of deposition with the substrate, it can be assessed with the percentage of infiltration of substrate's elements in the deposition. The dilution is experimentally predicted with the help of EDAX observed at the interjunction of deposition and substrate, wherein the percentage of Fe advocates the dilution percentage. The chromium boride (Cr_2B) distributed in the microstructure is assessed through XRD, wherein the peaks in counts corresponding to Cr_2B are quantified to include in the observation. The third objective is a microhardness value recorded from the hardness test.

3. Statistical computation

3.1. Grey Relational Analysis (GRA)

GRA is a versatile approach designed by Ju.Long [37] to facilitate a viable solution for the multi-objective problem. GRA meticulously handles a smaller number of data with discrete units. The minimum number of data with dubious and divergence are transformed into single data by using GRA. The multi-objective problem can be simplified into a single objective by giving a proper weightage and is referred to as Common Grey Relation Grade (CGRG) [38]. The diversified data with variations are streamlined into a single entity called the S/N ratio. The performance of the objective whether it is higher or lower can be approached by Taguchi's robust design. A collective assessment of the highest value of CGRG among all experimental trials signifies the set of optimal parameters. The present problem deals with five variables namely scanning speed, powder delivery, stan-off distance, current and boron weight percentage. The three different responses are dilution percentage, chromium boride and hardness. The quality characteristics of the responses are designated as higher dilution, higher chromium carbide formation and higher hardness. Therefore, as per Taguchi's robust design, the higher the better formulation is followed with appropriate relation shown in Fig. 2.

The various steps involved in the statistical manipulation of Grey Relational Grade (GRG) through Grey Relational Analysis (GRA) are depicted in Fig. 2

Table 6 illustrates the calculated values of S/N ratios, normalized S/Nratios, by using the appropriate equation prescribed in the

Table 1
Chemical constituents of deposited alloy with its variants.

Alloy Name	Elements (wt %)					
	Ni	Cr	Si	B	Fe	C
A1	76.4	13	3.2	2.5	4.5	0.4
A2	75.9	13	3.2	3	4.5	0.4
A3	75.4	13	3.2	3.5	4.5	0.4

Table 2
Chemical constituents of AISI 321 steel.

Elements	C	Mn	Si	P	S	Cr	Ni	Ti	Fe
Wt %	0.08	2	0.75	0.045	0.03	19	12	0.7	65.395

Table 3
Specifications of PTA welding resource.

Input supply	415 VAC/50–60 Hz/3 phase/4 wire
Installed power	17.65 kW
Current Range	20-400 Amps
Plasma gas	0-8.3 x 10^{-5} m^3/s
Shielding gas (Argon)	0-10.67 x 10^{-5} m^3/s
Carrier gas (powder gas)	0-25.05 x 10^{-5} m^3/s
Powder delivery	0.25–5 kg/h
Powder hopper capacity	700 cm^3
Tungsten electrode diameter	4.8 mm
Tungsten electrode length	175–300 mm
Torch grip dia	38 mm

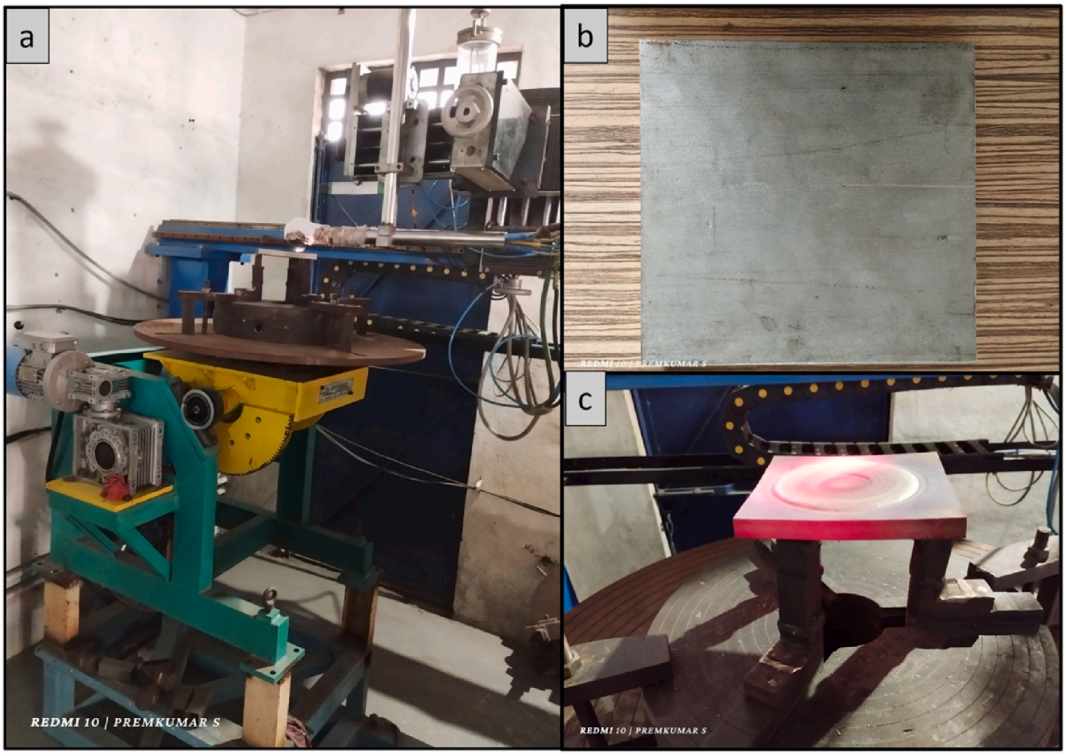

Fig. 1. Experimental constituents (a) PTA weld unit (b) AISI 321 substrate (c) Deposited specimen.

Table 4
Cladding parameters and their levels.

S.No	Parameter	Level 1 1	Level 2	Level 3
1	Scanning speed (mm/min)	200	400	600
2	Powder feed rate (gm/min)	6	8	10
3	Stand-off distance (mm)	7	14	21
4	Current (A)	80	100	120
5	Boron percentage (wt%)	2.5	3	3.5

Table 5
Combinations of experimental trials and their observations of objectives.

Experiment No	Scanning speed (mm/min)	Powder delivery (gm/min)	Stand-off distance (mm)	Current (A)	Boron percentage (wt %)	Dilution (%)	Chromium Boride (counts)	Hardness (HV)
1	200	6	7	80	2.5	15.4	234.7	376
2	200	8	14	100	3	19.3	247.8	413
3	200	10	21	120	3.5	17.3	254.5	401
4	400	6	7	100	3	22	251.2	398
5	400	8	14	120	3.5	34.4	295.5	804
6	400	10	21	80	2.5	18.5	238.7	400
7	600	6	14	120	3.5	24	258.3	596
8	600	8	21	80	2.5	21.4	242.3	409
9	600	10	7	100	3	28.2	245	436
10	200	6	21	100	3	22.3	247.8	462
11	200	8	7	120	3.5	28.4	263.4	567
12	200	10	14	80	2.5	20	239.7	398
13	400	6	14	80	2.5	26.7	261.7	543
14	400	8	21	100	3	25	254	444
15	400	10	7	120	3.5	29.8	268.9	623
16	600	6	21	120	3.5	28	272.4	698
17	600	8	7	80	2.5	21	261.8	400
18	600	10	14	100	3	23	259	435

GRA procedure. Table 7 depicts the manipulated values of Grey relational coefficients and common grey relational grades.

3.2. Machine learning algorithm

Machine learning algorithms (MLA) are versatile in predicting the best possible one among the pool of voluminous data. Pandas is a data manipulation library and sci-kit-learn is a machine learning library in Python used to generate the code [39]. The training and testing of data are executed by the exclusive module called the train_test_split module. The majority (80 %) of the data are used for training and a minority (20 %) are used for testing. The responses' dilution, microstructure and hardness are designated as target variables and their performance characteristics are ascribed as high. A supervised learning algorithm, Random Forest Regressor (RFR) is pressed into predictive analysis to predict an optimal set of PTAW parameters and wt.% of boron along with the significance of each parameter over the responses. RFR is an elementary algorithm that works on both large and small datasets with notable accuracy. RFR proliferates a huge decision tree from which the prediction happens [40]. A leaf approach is followed to counter the overfitting issues. One branch (predictands) after the split is considered as one decision tree, and the branches are split into binary predictors until it reach a single node and is called leave. The average value of the predictions performed by the decision trees is considered to be a final prediction as given below

$$\widehat{y} = \frac{1}{N}\sum_{i=1}^{N} y_i$$

3.3. Optimal combinations of PTAW parameters and wt% of boron

The optimal set of parameters and wt.% of boron to yield a maximum dilution, maximum chromium boride (higher peaks), and maximum hardness is predicted statistically through GRA is shown in Fig. 3. It is identified that 400 mm/min of scanning speed, 8 gm/min of powder delivery, 14 mm of stand-off distance, 12 A of current and 3.5 wt % of boron is found to be the optimal set of experiments to achieve the best performance characteristics of the responses considered. A similar prediction has been realized through the results earned using the machine learning algorithm as shown in Fig. 4 (a). Accuracy of the prediction executed by MLA is validated through a scatter plot shown in Fig. 4 (b), wherein the line of best fit is observed between actual CGRG and predicted CGRG. Indeed, the statistical approach GRA and supervised algorithm-based RFR, indicate Experiment No.5 as the best experiment to yield higher dilution, higher chromium boride, and higher hardness. Fig. 5(a) and (b) & **(c)** illustrate the significance of each parameter in mitigating the responses like dilution, microstructure, and hardness. The current is the most significant parameter for better dilution at the cladding interface, followed by the scanning speed. For the higher peak of chromium boride and higher hardness, the weight percentage of boron is found to be the most paramount parameter followed by the current. The MLA-based RFR algorithm manifests the insignificance of powder delivery and stand-off distance.

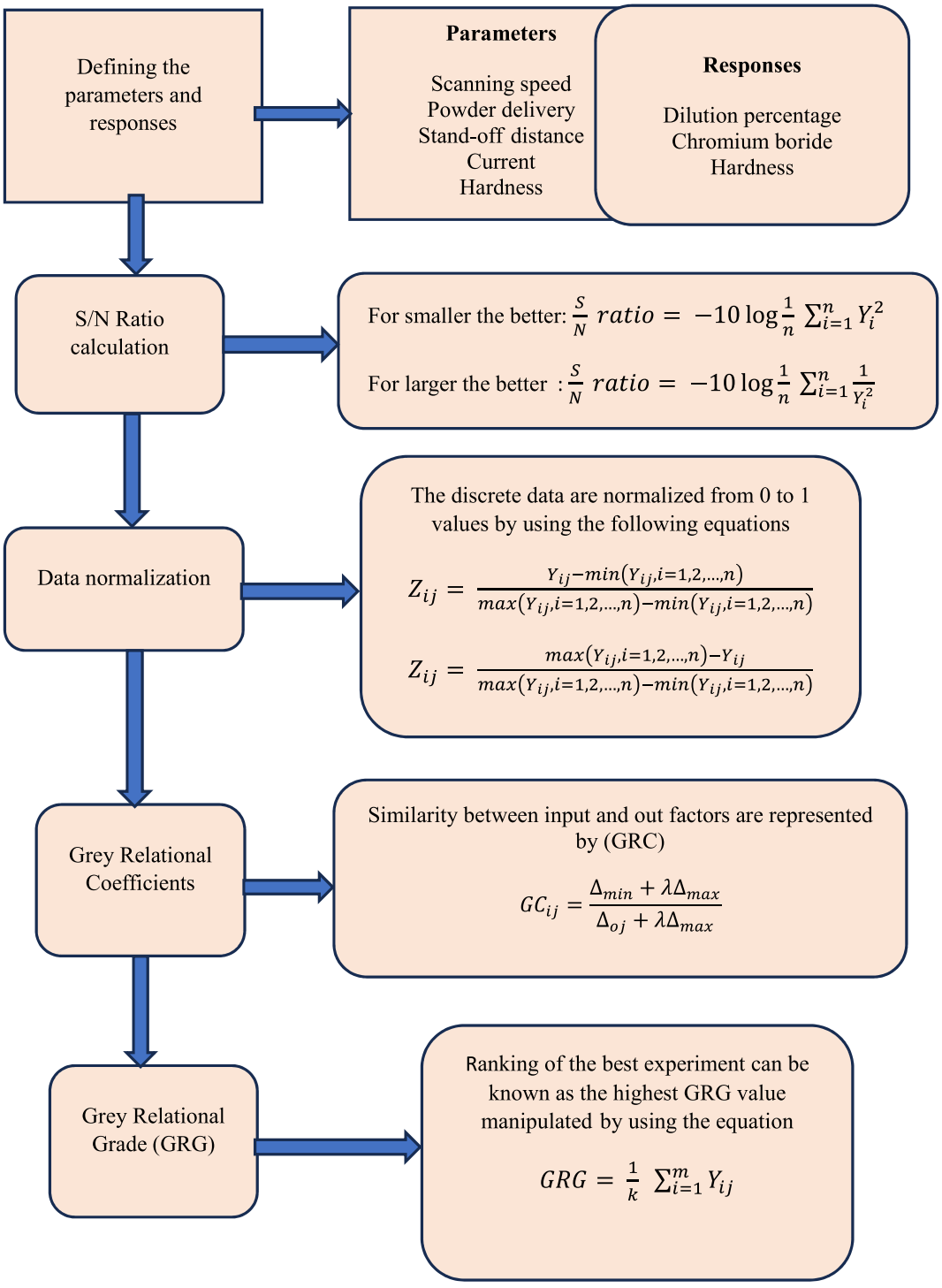

Fig. 2. Schematic procedures of Grey Relational Analysis.

4. Results and discussion

4.1. Effect of cladding parameters on dilution

4.1.1. Effect of scanning speed

Fig. 6(a) and (b) and 7 (a) & (b) show the elemental composition obtained from the EDAX conducted for experiments No.5 and No.1

Table 6
Calculated values of S/N and normalized S/N ratios.

S/N Ratio			Normalized S/N ratio		
Dilution %	Microstructure	Hardness	Dilution %	Microstructure	Hardness
36.30	59.96	64.06	0.00	0.00	0.00
38.26	60.43	64.87	0.72	0.76	0.88
37.31	60.67	64.62	0.86	0.65	0.92
39.40	60.55	64.55	0.56	0.70	0.93
43.28	61.96	70.66	1.00	1.00	1.00
37.90	60.11	64.59	0.77	0.93	0.92
40.16	60.80	68.06	0.45	0.58	0.39
39.16	60.24	64.79	0.59	0.86	0.89
41.56	60.34	65.34	0.25	0.81	0.81
39.52	60.43	65.85	0.54	0.76	0.73
41.62	60.97	67.62	0.24	0.50	0.46
38.57	60.15	64.55	0.67	0.91	0.93
41.08	60.91	67.25	0.31	0.53	0.52
40.51	60.65	65.50	0.40	0.66	0.78
42.04	61.14	68.44	0.18	0.41	0.34
41.50	61.26	69.43	0.26	0.35	0.19
39.00	60.91	64.59	0.61	0.52	0.92
39.79	60.82	65.32	0.50	0.57	0.81

Table 7
Calculated Grey Relational Coefficients (GRC) and Common Grey relational Grade (GRG).

Experiment No	Grey relational coefficients			CGRG
	Dilution	Microstructure	Hardness	
1	1.00	1.0000	1.0011	0.33
2	0.64	0.6791	0.8026	0.71
3	0.78	0.5867	0.8559	0.74
4	0.53	0.6285	0.8706	0.68
5	0.33	0.3329	0.3334	1.00
6	0.69	0.8718	0.8607	0.81
7	0.48	0.5454	0.4522	0.49
8	0.55	0.7830	0.8194	0.72
9	0.40	0.7280	0.7201	0.62
10	0.52	0.6791	0.6489	0.62
11	0.40	0.4991	0.4807	0.46
12	0.61	0.8451	0.8706	0.77
13	0.42	0.5136	0.5086	0.48
14	0.45	0.5926	0.6961	0.58
15	0.38	0.4580	0.4295	0.42
16	0.40	0.4356	0.3806	0.41
17	0.56	0.5127	0.8607	0.65
18	0.50	0.5385	0.7233	0.59

respectively. The elemental mapping results delineate the supremacy of Fe in Experiment No.5 as 68.59 %, and deficiency in Experiment No. 1 as 34.88 %. The increased dilution is realized from Experiment No.5 as it records a higher Fe content of 96.6 % than Experiment No.1. The infiltration of Fe into the substrate authenticates the dilution and in turn good bonding of the deposition. At a higher level of scanning speed (600 mm/min), dilution is observed to be lesser to the scale of 34.88 %. A higher level of scanning speed reduces both the energy deposition and powder deposition per length [35].

At higher scanning speeds, the insufficient time to interact with the powder by the plasma leaves the deposition not to melt properly. The improper melting of both substrate and powder yields a lower dilution. The cross-sectional area of the deposited layer is also lesser at higher scanning speeds reported by the researchers [35] owing to the lesser energy and powder deposition per length. Fig. 6(a) and (b) assures the higher infiltration of Fe obtained at lower scanning speed and it reflects the higher dilution. The higher dilution is measured with the quantity of the chief element present in the substrate infiltrated through the deposition. The previous researchers claimed a higher dilution with a record of 39 % of Fe infiltrated and detected through EDAX [34]. The optimal scanning speed of 400 mm/min ensures better dilution which is attributed to the homogenous melting of both substrate and powder. At slow scanning speed, plasma has sufficient time to interact with powder and substrate, wherein proper melting and better dilution. The researchers reported A similar finding [41] when they deposited AISI 316l powder on carbon steel (AISI A105). The report concluded that the increase in dilution was attained at low levels of scanning speed.

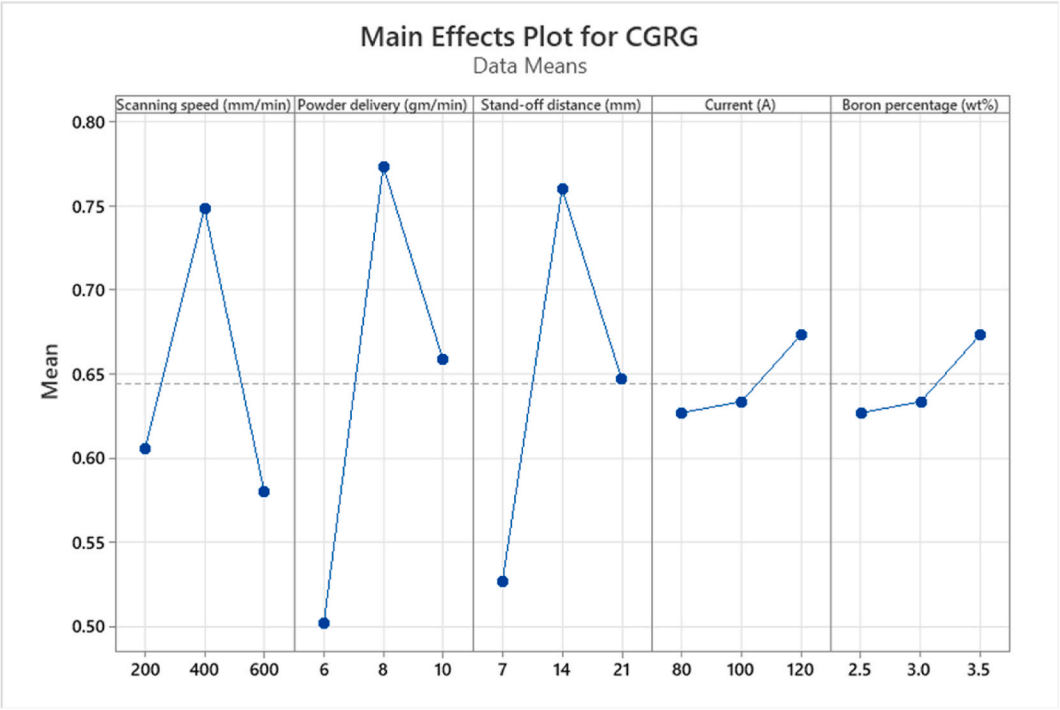

Fig. 3. The optimal level of each parameter suggested by the main effect plot.

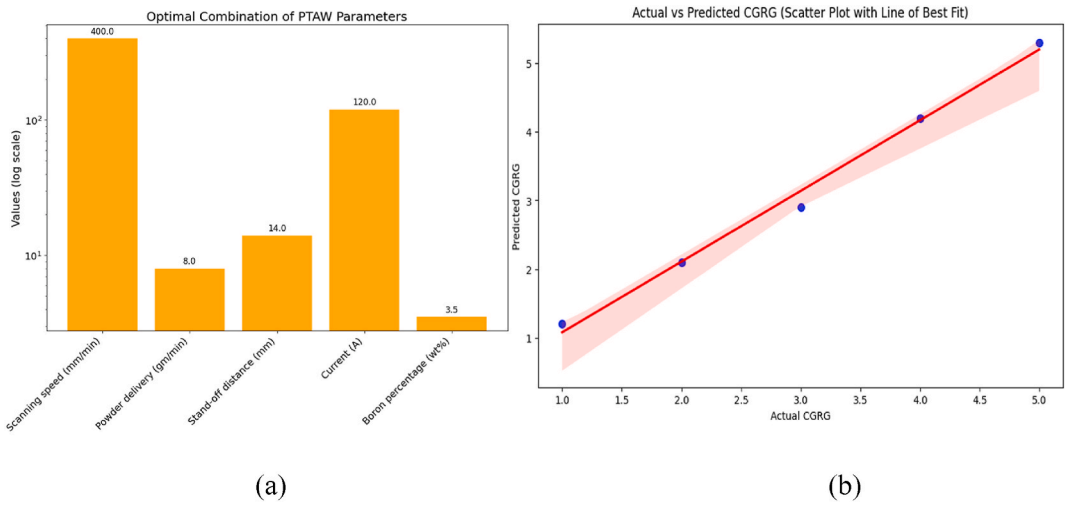

Fig. 4. Prediction of optimal parameters through MLA (a) Predicted set of optimal parameters (b) Line of best fit.

4.1.2. Effect of powder delivery

The powder delivery influences the dilution percentages because the total heat energy supplied by the plasma is divided into two segments, wherein part of the energy is supplied to the powder and the remainder to the substrate. The higher quantity of powder delivery absorbs more amount of heat energy causing the substrate to improperly melt with insufficient heat. However, the lesser powder delivery has the opposite effect resulting in larger heat to the substrate and lesser heat to the powder. Hence the higher and lesser powder delivery causes scarce heat to the substrate and powder respectively, thereby challenging the dilution. The experiments belonging to higher and medium powder delivery are depicted in Fig. 6(a) and (b) and Fig. 7(a) and (b) which authenticates the richer and poorer infiltration of Fe to showcase the performance of dilution.

4.1.3. Effect of stand-off distance

The stand-off distance impacts the plasma arc density. The higher the stand-off distance lower the plasma arc density and vice

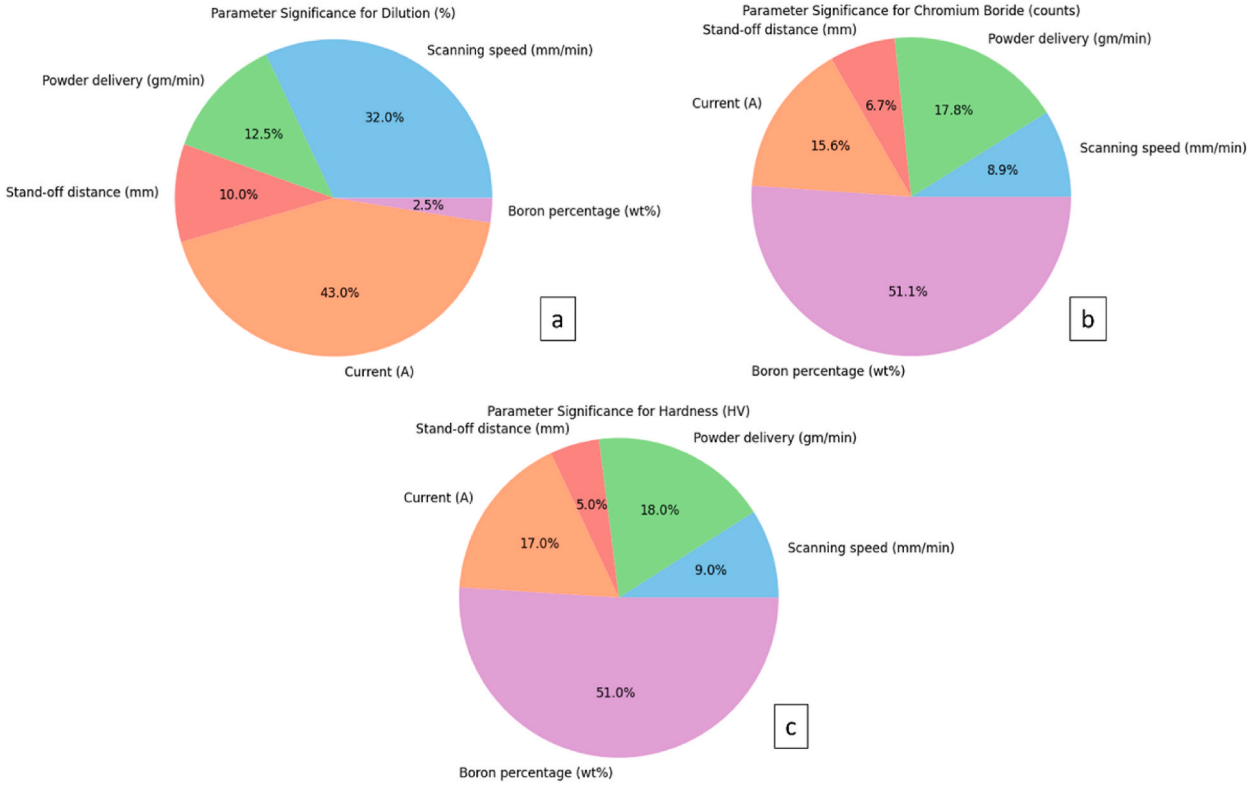

Fig. 5. Prediction of the significance of parameter (a) for dilution (b) for Chromium boride formation (c) Hardness.

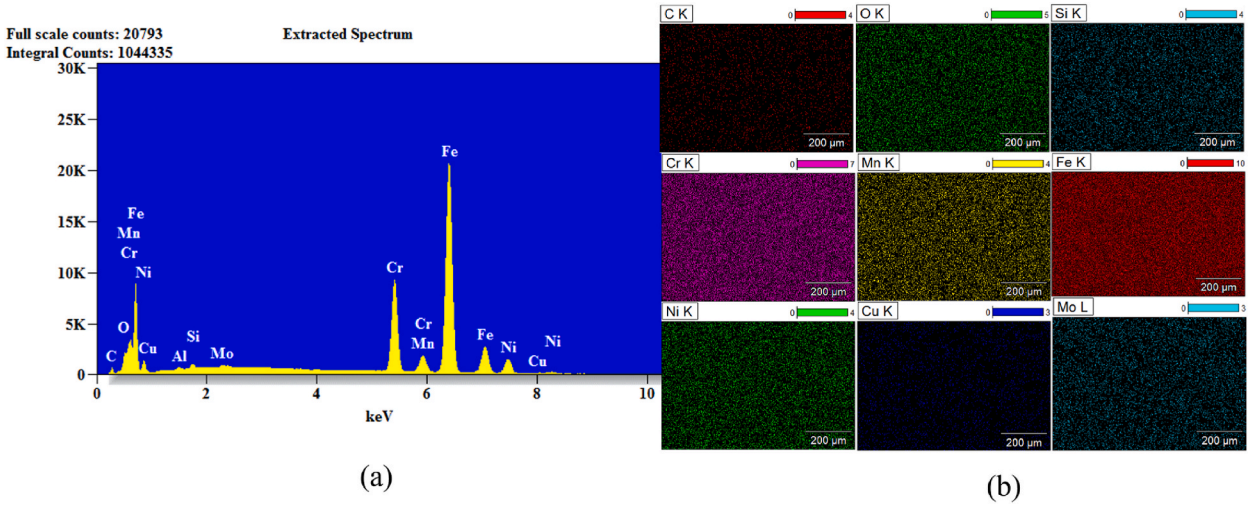

Fig. 6. Elemental mapping for Experiment No.5 (a) EDAX analysis results (b) Elements and their weightage.

versa. The inadequate heat source caused by the low-dense plasma arc supplied at a longer stand-off distance induces a poorer percentage of dilution. The result shows in Fig. 6(a) and (b) authenticate the better dilution recorded for the experiment with a lesser stand-off distance. At a lesser stand-off distance, the density of the plasma arc increases and assures more heat to melt both powder and substrate resulting in better dilution.

4.1.4. Effect of current

The higher current ensures higher energy deposition per length through more heat intensity and arc beam density. A higher percentage of Fe penetration is detected for the experiments shown in Fig. 6(a) and (b) conducted with a higher level of current. The

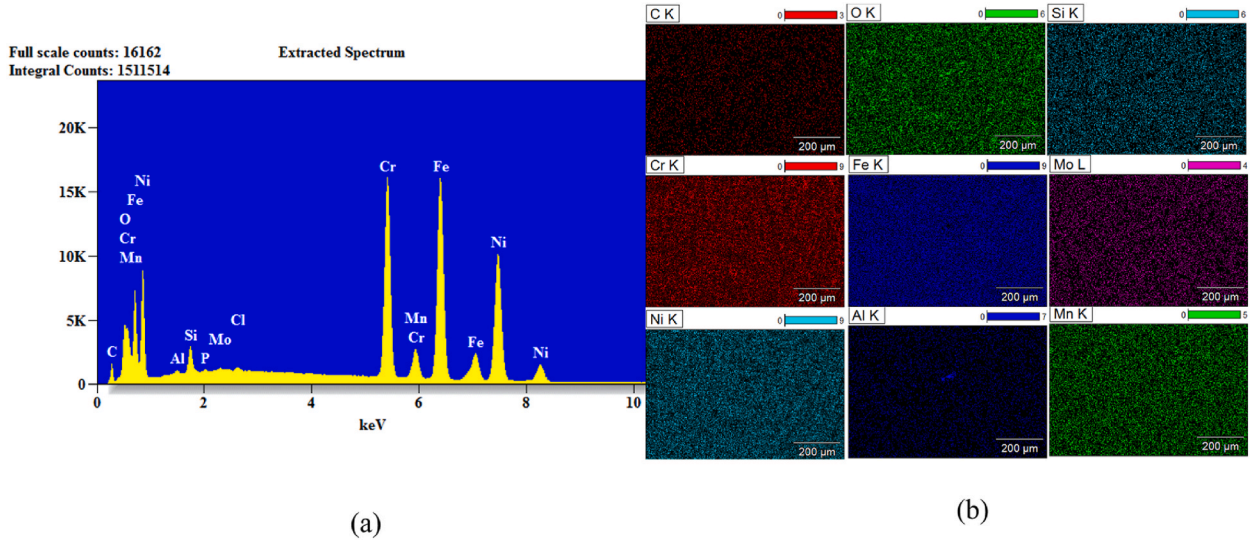

Fig. 7. Elemental mapping for experiment No.1 (a) EDAX analysis results (b) Elements and their weightage.

scarce heat and weak plasma arc density delivered at a lower level of current yield a poorer dilution which is obtained from experiment No.1. The poorer dilution obtained from the lower level of current is further endorsed by Fig. 7(a) and (b). A similar investigation was executed by the researchers [35] to deposit SS 304L powders on SS 316 plates through the PTAW process. The concise report concluded that the moderate level of (300 mm/min) of scanning speed, lower level of powder delivery (6 gm/min) and lower level of stand-off distance (6 mm) yielded a maximum dilution of 25 %, 37.5 % and 20 % respectively.

4.2. Effect of process parameters on microstructure and boride formation

The presence of chromium boride is determined through XRD analysis. The higher the peak, the higher the chromium boride. Apart from the considered process parameters, to affect the chromium chloride formation, the powder composition itself influences the boride formation. The XRD results obtained from higher and lower levels of boron percentages in the powder are shown in Fig. 8(a) and (b) respectively**.** It is witnessed from the results that the higher peaks of chromium boride are evident for the higher composition of boron in the powder.

4.2.1. Effect of scanning speed

PTAW parameters highly influence the development of microstructure and its integrity. The scanning speed mitigates the heat energy and its exposure to the powder and substrate. The higher level of scanning speed limits the heat energy as the interaction time of the plasma beam with the substrate is minimal. The restriction in heat energy offered by a faster scanning speed leaves the deposition without the formation of significant HAZ. The microstructure developed through a higher scanning speed delineates fine grain structure. Fig. 9(a) and (b) shows the macro observation of microstructure obtained through an optical microscope for experiments No.5 and No.1 respectively.

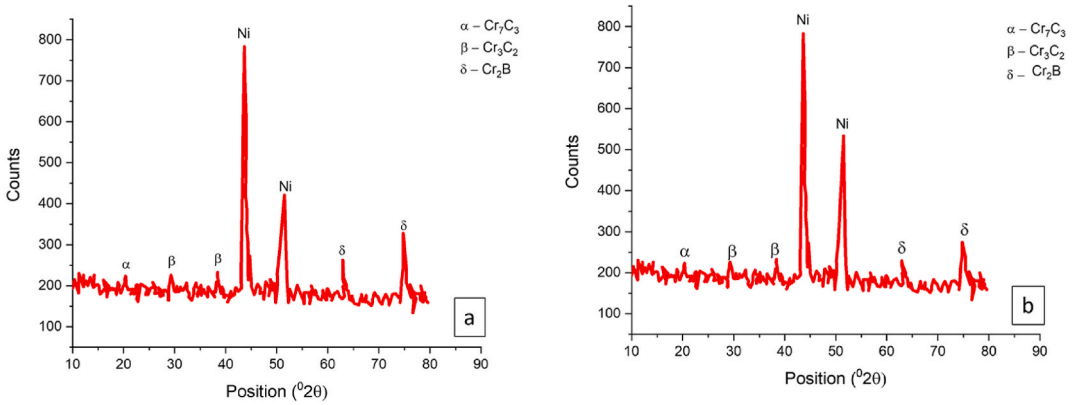

Fig. 8. XRD Results (a) at Higher Boron content (b) at lower boron content.

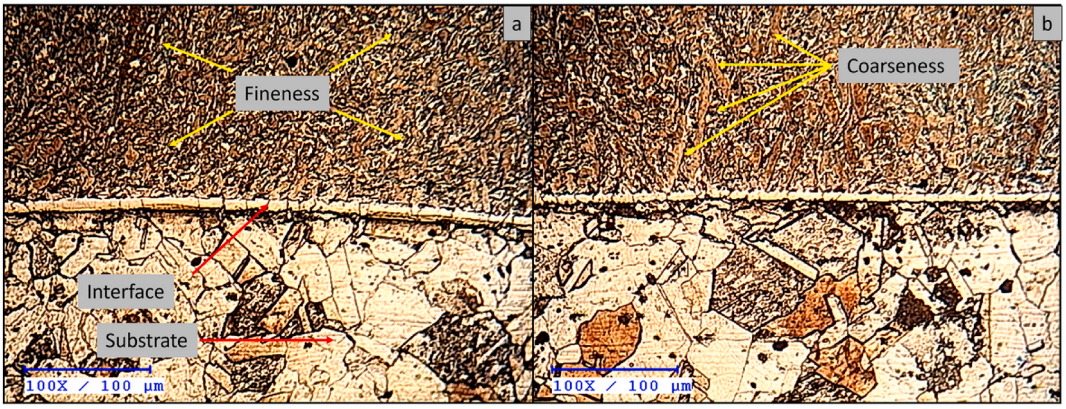

Fig. 9. Macrographs of the deposited interface (a) From experiment No.5 (b) From experiments No.1.

The fine-grain structure developed at a higher scanning speed is witnessed from Fig. 9 (a). Conversely, the coarser grain structure with dendrite formation developed at a lower scanning speed is visible from Fig. 9 (b). At low scanning speed, sustained interaction of the plasma beam with the powder and substrate, induces the HAZ. HAZ ensures high temperature and promotes grain growth which leads to a coarser grain structure as depicted in Fig. 9 (b).

4.2.2. Effect of powder delivery

The quantity of powder delivered considerably influences the microstructure. The lesser powder volume absorbs less heat energy and major heat energy is diverted to the substrate. The higher heat energy causes grain growth to settle down as a coarser grain structure. The higher powder volume retards the formation of HAZ, thereby helping to form the fine-grain structure. It is noteworthy that the abundant volume of powders experiences inhomogeneity in melting which leads to the inferior deposition. The fine grain structure developed for experiment No.5 is driven by a medium powder volume of 8 gm/min.

4.2.3. Effect of stand-off distance

The distance between the substrate and the cladding nozzle determines the stand-off distance. The increased stand-off distance minimizes the interaction of heat energy with the substrate leaving the powders as half-melt. The decreased stand-off accelerates the heat energy and higher heat energy contributes to the formation of HAZ. The moderate level of stan-off distance ensures the homogenous melting of powders and gets rid of HAZ formation. Fig. 9 (a) endorses the formation of fine grain structure induced at a moderate stand-off distance of 14 mm.

4.2.4. Effect of current

The higher level of current discharges more heat and widens the HAZ, whereas the lower level of current discharges insufficient heat to melt both powder and substrate. Theoretically, HAZ and high temperatures retain the grain growth to form a coarser grain structure. However, the optimal combination of individual parameters mitigates the microstructure in a finer way as depicted in Fig. 10 (b).

Fig. 10 (a) and **(b)** illustrate the SEM micrographs observed at the interface of the deposited layer. A lesser number of grains per unit

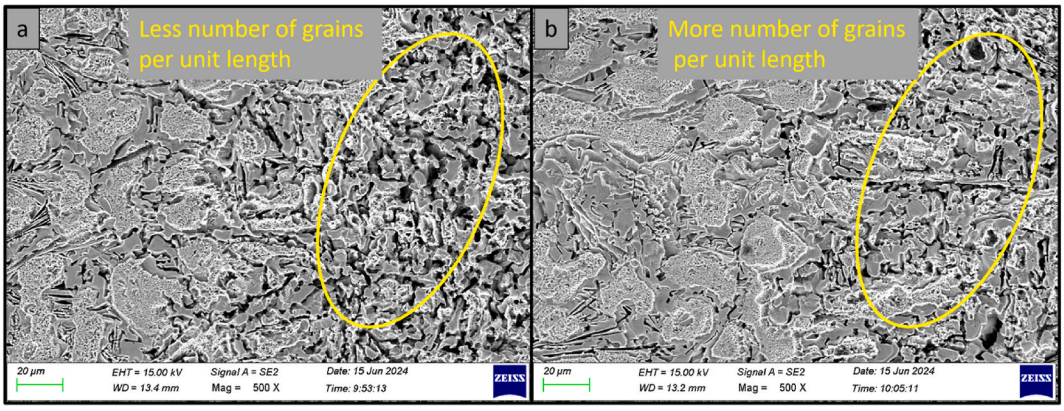

Fig. 10. Micrographs (a) at a lower current level (b) at a higher current level.

length is witnessed at lower levels of current from experiment No.1. However, more number of grains per unit length is observed for higher levels of current supplemented by experiment No.5. It is interesting to record the peculiar behaviour of higher level of current in demonstrating a finer grain structure along with higher content boron. Usually, the higher level of current retains the grain growth as the temperature maintains at its peak. That is why, a coarser grain size was observed at a higher current by the researchers [42], while they attempted to deposit Ni–Cr–B–Si alloy reinforced with tungsten carbide. However, interestingly, the report explored that the increased hardness was achieved due to the higher dilution at a higher current, wherein, more tungsten carbide formation was observed. Nevertheless, the coarser grain size was reported. Similarly, in the present work, the effect of coarse grain size formation is suppressed due to the higher inclusion of known grain refiner boron. The inclusion of boron in higher levels mitigates the grain growth to form a finer grain structure, even at high temperatures. Hardness is a dependent property of boride formation, a higher boride formation can impart a high hardness.

5. Conclusions

The present work targets the development of wear-resistant surfaces for high-temperature applications such as exhaust systems, combustion chamber liners, turbine blades, high-performance braking pads, etc. The thorough experimental study, followed by statistical and MLA-based prediction to identify a set of ideal PTAW process parameters and powder composition to obtain improved dilution, microstructure, and hardness, yields the following constructive conclusions.

1. The implementation of the statistical technique GRA and machine learning technique RFR invariably identifies experiment No. 5 as an ideal experiment.
2. Microstructural analyses conducted through SEM reveal the finer grain size evolved within the deposition for the ideal experiment No.predicted from analytical and soft computing, in contrast, coarser grains evolved for non-optimal trail, i.e experiment No.1.
3. 400 mm/min scanning speed, 8 gm/min powder delivery, 14 mm stand-off distance, and 120 A current are optimal sets of PTAW parameters along with 3.5 % boron content in powder composition to acquire a higher dilution, chromium boride deposition and hardness.
4. The RFR machine learning algorithm reveals that the current is the predominant parameter followed by the scanning speed to achieve a better dilution at the cladding interface. Consequently, the weight percentage of boron in the powder composition is the chief parameter followed by the current to dictate the deposition of chromium boride, microstructure and hardness.
5. The higher peak of chromium boride ensures the extreme hardness of 804 HV for experiment No.5 which is 113.8 % higher than the hardness developed from experiment No.1. Therefore, the deposition is the right candidate for high-temperature wear-resistant applications.
6. The attainment of dilution of 34.4 % exhibits the rigid bonding of the deposited layer over the substrate.

Funding statement

The authors did not receive support from any organization for the submitted work.

6. Nomenclature

Y_i	–	Response values of ith trial
Z_{ij}	–	Normalized S/N ratio for ith^{trial}
Y_{ij}	–	S/N ratio for ith^{trial}
GC_{ij}	–	Grey relation coefficient for ith^{trial}
Δ_{min}	–	Maximum deviation sequence
Δ_{max}	–	Minimum deviation sequence
λ	–	Distinguished sequence
Δ_{ij}	–	Deviation sequence for ith^{trial}
γ_i	–	Grey relation grade for ith^{trial}

CRediT authorship contribution statement

Venkatesh Chenrayan: Writing – original draft, Validation, Formal analysis. **Kiran Shahapurkar:** Methodology, Formal analysis, Data curation, Conceptualization. **Chandru Manivannan:** Software, Project administration, Methodology, Formal analysis. **L. Rajesh Kumar:** Writing – review & editing, Validation, Supervision. **Sivakumar Nadarajan:** Validation, Software. **Rajesh sharma:** Validation, Software. **R. Venkatesan:** Supervision, Project administration.

Declaration of competing interest

The authors declare the following financial interests/personal relationships which may be considered as potential competing interests:

L. Rajeshkumar is one of the author of the manuscript and is an Associate Editor of Materials Science Section. If there are other

authors, they declare that they have no known competing financial interests or personal relationships that could have appeared to influence the work reported in this paper.

Acknowledgement

The authors express their appreciation and acknowledgement to the administration of the Alliance Univesity, Bengaluru, for their extended support for this research work.

References

[1] J.X. Fang, et al., Microstructure evolution and deformation behavior during stretching of a compositionally inhomogeneous TWIP-TRIP cantor-like alloy by laser powder deposition, Materials Science and Engineering: A 847 (2022) 143319.
[2] Z. Zhang, et al., Effects of solder thickness on interface behavior and nanoindentation characteristics in Cu/Sn/Cu microbumps, Weld. World 66 (5) (2022) 973–983.
[3] R. Ranjan, A.K. Das, Protection from corrosion and wear by different weld cladding techniques: a review, Mater. Today: Proc. 57 (2022) 1687–1693.
[4] J. Wang, et al., Evolution of crystallographic orientation, precipitation, phase transformation and mechanical properties realized by enhancing deposition current for dual-wire arc additive manufactured Ni-rich NiTi alloy, Addit. Manuf. 34 (2020) 101240.
[5] X. Xu, et al., Effect of undercooling on microstructure evolution of Cu based alloys, J. Alloys Compd. 935 (2023) 167998.
[6] L. Zhu, et al., Recent research and development status of laser cladding: a review, Opt Laser. Technol. 138 (2021) 106915.
[7] Y. Zhao, Y. Sun, H. Hou, Core-shell structure nanoprecipitates in Fe-xCu-3.0Mn-1.5Ni-1.5Al alloys: a phase field study, Prog. Nat. Sci.: Mater. Int. 32 (3) (2022) 358–368.
[8] X. Liu, et al., Studies on high power laser cladding Stellite 6 alloy coatings: metallurgical quality and mechanical performances, Surf. Coating. Technol. 481 (2024) 130647.
[9] J. Amado, et al., Laser cladding of tungsten carbides (Spherotene®) hardfacing alloys for the mining and mineral industry, Appl. Surf. Sci. 255 (10) (2009) 5553–5556.
[10] S. Aghili, et al., Microstructure and oxidation behavior of NiCr-chromium carbides coating prepared by powder-fed laser cladding on titanium aluminide substrate, Ceram. Int. 46 (2) (2020) 1668–1679.
[11] N. Jeyaprakash, C.-H. Yang, K. Ramkumar, Microstructure and wear resistance of laser cladded Inconel 625 and Colmonoy 6 depositions on Inconel 625 substrate, Appl. Phys. A 126 (6) (2020) 455.
[12] C. Yuhua, et al., Investigation of welding crack in micro laser welded NiTiNb shape memory alloy and Ti6Al4V alloy dissimilar metals joints, Opt Laser. Technol. 91 (2017) 197–202.
[13] Y. Chen, et al., Effects of post-weld heat treatment on the microstructure and mechanical properties of laser-welded NiTi/304SS joint with Ni filler, Materials Science and Engineering: A 771 (2020) 138545.
[14] J. Tuominen, et al., Microstructural and abrasion wear characteristics of laser-clad tool steel coatings, Surf. Eng. 32 (12) (2016) 923–933.
[15] Y. Liu, et al., Research on microstructure and properties of Ti-based coating prepared by laser cladding on titanium alloy: simulation and experiment, J. Mater. Res. Technol. 20 (2022) 3667–3682.
[16] L. Shao, et al., Why do cracks occur in the weld joint of Ti-22Al-25Nb alloy during post-weld heat treatment? Frontiers in Materials 10 (2023) 1135407.
[17] N.V. Rao, G.M. Reddy, S. Nagarjuna, Weld overlay cladding of high strength low alloy steel with austenitic stainless steel–structure and properties, Mater. Des. 32 (4) (2011) 2496–2506.
[18] S. Amin, H. Panchal, A review on thermal spray coating processes, transfer 2 (4) (2016) 556–563.
[19] J. Jiang, et al., Interfacial microstructure and mechanical properties of stainless steel clad plate prepared by vacuum hot rolling, J. Iron Steel Res. Int. 25 (2018) 732–738.
[20] X. Guo, et al., Interface and performance of CLAM steel/aluminum clad tube prepared by explosive bonding method, Int. J. Adv. Des. Manuf. Technol. 82 (2016) 543–548.
[21] D.-f. Mo, et al., A review on diffusion bonding between titanium alloys and stainless steels, Adv. Mater. Sci. Eng. 2018 (1) (2018) 8701890.
[22] H.A. Khan, et al., Roll bonding processes: state-of-the-art and future perspectives, Metals 11 (9) (2021) 1344.
[23] A.N.S. Appiah, et al., Powder plasma transferred arc welding of Ni-Si-B+ 60 wt% WC and Ni-Cr-Si-B+ 45 wt% WC for surface cladding of structural steel, Materials 15 (14) (2022) 4956.
[24] L. Zunake, V. Kalyankar, On the performance of weld overlay characteristics of Ni–Cr–Si–B deposition on 304 ASS using synergetic pulse-GMAW process, Sci. Technol. Weld. Join. 26 (2) (2021) 106–115.
[25] M. Adamiak, et al., Experimental comparison of laser cladding and powder plasma transferred arc welding methods for depositing wear-resistant NiSiB+ 60% WC composite on a structural-steel substrate, Materials 16 (11) (2023) 3912.
[26] S. Wang, et al., The design of low-temperature solder alloys and the comparison of mechanical performance of solder joints on ENIG and ENEPIG interface, J. Mater. Res. Technol. 27 (2023) 5332–5339.
[27] Y. Huang, X. Zeng, Investigation on cracking behavior of Ni-based coating by laser-induction hybrid cladding, Appl. Surf. Sci. 256 (20) (2010) 5985–5992.
[28] J. Xie, et al., Microstructure and mechanical properties of Mg–Li alloys fabricated by wire arc additive manufacturing, J. Mater. Res. Technol. 29 (2024) 3487–3493.
[29] Z. Yang, et al., An additively manufactured heat-resistant Al-Ce-Sc-Zr alloy: microstructure, mechanical properties and thermal stability, Materials Science and Engineering: A 872 (2023) 144965.
[30] I. Hemmati, et al., Phase formation and properties of vanadium-modified Ni–Cr–B-Si–C laser-deposited coatings, J. Mater. Sci. 48 (2013) 3315–3326.
[31] C. Sudha, et al., Microchemical and microstructural studies in a PTA weld overlay of Ni–Cr–Si–B alloy on AISI 304L stainless steel, Surf. Coating. Technol. 202 (10) (2008) 2103–2112.
[32] C. Zhang, et al., Plasma transferred arc cladding of Ni-Cr-B-Si coating on copper substrate, Mater. Lett. 14 (2022) 100137. X.
[33] T.-g. Guan, et al., Microstructure and wear resistance of ZrC-ZrB 2/Ni composite coatings prepared by plasma transferred arc cladding, Mater. Res. 22 (2019) e20180781.
[34] I. Hemmati, V. Ocelík, J.T.M. De Hosson, Dilution effects in laser cladding of Ni–Cr–B–Si–C hardfacing alloys, Mater. Lett. 84 (2012) 69–72.
[35] S. Mandal, et al., An experimental investigation and analysis of PTAW process, Mater. Manuf. Process. 30 (9) (2015) 1131–1137.
[36] L. Shao, et al., Influence of heat treatment Condition on the microstructure, microhardness and corrosion resistance of Ag-Sn-in-Ni-Te alloy wire, Materials 17 (11) (2024) 2785.
[37] D. Ju-Long, Control problems of grey systems, Syst. Control Lett. 1 (5) (1982) 288–294.
[38] H. Biratu, et al., Effect of Caesalpinia decapetala on the Dry Sliding wear behavior of Epoxy Composites, International Journal of Polymer Science 2023 (1) (2023) 9379277.
[39] S.G. Fashoto, et al., Implementation of machine learning for predicting maize crop yields using multiple linear regression and backward elimination, Malaysian Journal of Computing (MJoC) 6 (1) (2021) 679–697.

[40] J. Graw, W. Wood, B. Phrampus, Predicting global marine sediment density using the random forest regressor machine learning algorithm, J. Geophys. Res. Solid Earth 126 (1) (2021) e2020JB020135.
[41] J.A. Robert Jayachandran, N. Murugan, Investigations on the influence of surfacing process parameters over bead properties during stainless steel cladding, Mater. Manuf. Process. 27 (1) (2012) 69–77.
[42] E. Badisch, M. Kirchgaßner, Influence of welding parameters on microstructure and wear behaviour of a typical NiCrBSi hardfacing alloy reinforced with tungsten carbide, Surf. Coating. Technol. 202 (24) (2008) 6016–6022.